The Manufacture of Continuous Electrodes using Paste Briquettes

ELKEM

September 5, 1997

1 Introduction

This problem was brought to the 1997 European Study Group with Industry at the University of Bath by Svenn Anton Halvorsen of Elkem ASA, Kristiansand, Norway. It concerns a method for manufacturing continuous electrodes which are used in electric smelting furnaces. The purpose of such electrodes (of which there are a number of different types - see below for further details) is to conduct currents of up to 150,000 Amps to the centre of a smelting furnace thereby providing the energy required to produce calcium carbide or ferro alloys. During a typical process the electrodes are consumed at a rate of about 0.5m/day and are normally charged by adding large (typically 1m high cylinders of diameter up to 1m) blocks of raw material to the top of the electrode. Central to the issues that will be discussed in this study is the raw material that makes the electrodes, which will hereafter be referred to as 'paste'. This is a mixture of binder (tar and pitch) and calcined anthracite. The anthracite particles are present in a wide size range and may have typical dimensions of anything between a number of microns and a few millimetres. Solid at room temperature, the paste starts to soften at around 50 C and flows when the temperature reaches 80 C. The effective viscosity of standard Søderberg paste reaches a minimum value at about 200-250C, after which it begins to increase with temperature as the tar and pitch begin to react and bind. At around 400 C the paste viscosity begins to increase rapidly and the electrode 'bakes', becoming solid at 500C. At 1000 C the bake is complete. During the baking its strength has increased greatly and its thermal conductivity has improved by a factor of between two and four; the electrical conductivity has increased by orders of magnitude, transforming an insulator into a conductor.

At present, the self-baking continuous electrode is used successfully throughout the world (for further details see Innvaer (1992)). One important aspect of the procedure, however, concerns the recharging of the electrode. Presently large sections are used to replenish the electrode above the furnace. Although the charging of a Søderberg electrode (see previous study group reports for details of the basics of such electrodes) is a fairly easy process, for the Persson electrode (see section 4 for a general description of this electrode) it is not possible to apply cylinders for replenishment. Only one alternative to section replacement has seriously been considered; instead of using large sections of paste for electrode replenishment, 'briquettes' (small bricks of paste of typical dimensions $10 \times 6 \times 4$ cm) may simply be added to the top of the electrode. As the briquettes

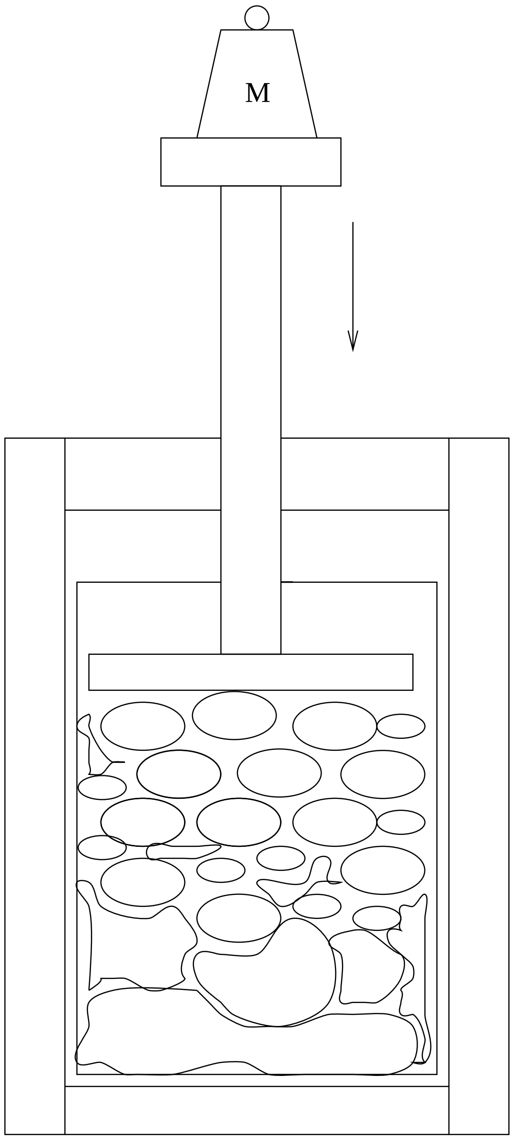

Figure 1: Experimental device for measurement of briquette density

gradually progress downwards towards the furnace, the increase in temperature causes them to flow, the air in the gaps between the briquettes is expelled, and a self-baking electrode is formed.

Full scale electrodes charged with briquettes have been tested and are currently in operation; however, a great deal of further information is required concerning this new process. Some initial experiments have taken place using apparatus similar to that shown in schematic form in figure 1. The piston in the device is loaded with a mass M ($M = 31$ kg in the Elkem experiments carried out so far) and the experiment takes place in a low-powered oven where the temperature is held constant at about 100 C. The piston and the sides of the container are perforated so that air can easily escape but molten paste cannot. Over a period of 5-6 hours the position of the top of the piston is monitored, allowing the effective (i.e. paste + air) paste density to be measured.

1.1 Alternative Electrodes for Silicon Production

Since the early part of this century, the Søderberg electrode has been the only continuous self baking electrode available for calcium carbide and ferroalloy production. Although many technical advances have taken place to allow increases in size and efficiency, the basic design has remained almost unchanged since the first Søderberg electrode was used in 1919. For processes (manufacture of calcium carbide, ferro alloys, for instance) where the product may contain some iron, there is still no alternative to the Søderberg electrode. The fins and casing of the electrode typically introduce some 0.1-1.0% iron into the end product. If silicon were the end product, about 1% iron would be introduced, an unacceptably high level. In recent years, therefore, a number of new types of electrode have been proposed with silicon production in mind. Two new designs that have attracted particular interest have become known, after their originators, as the 'Persson' and 'Bruff' electrodes.

In the Persson design, a central graphite carbon core is surrounded by paste in a stationary casing. Some device holds the core section in place and allows it to slip. During processing, the core is fused into the paste as it is carbonised. The great advantage of this design is that, unlike the Søderberg system where the metal electrode casing is present during the whole process and is consumed in the furnace together with the electrode, here the emerging carbon has no case. This is crucial for the production of silicon where the presence and subsequent consumption of the metal electrode casing would otherwise introduce too much iron into the furnace.

The Bruff electrode uses a specialised heating zone to melt and bake the paste. Heat is provided by propane burners and some of the hydrocarbons escaping from the baking paste are also used to power the process. Once again, the main purpose of this arrangement is to produce a caseless electrode.

Space does not permit a full description of the details and advantages of these new types of electrode, but more information may be found in Fulgenzi (1992) and Persson & Fava (1991) where many additional advantages are claimed for the new designs.

1.2 Questions for the Study Group

The purpose of the present study was to address questions relating to both the experiment and full-sized electrodes. Amongst other things, Elkem wish to know

- Can a mathematical model be formulated for the experiment which gives reasonable agreement with results already obtained ?

- What are the important parameters in the problem, and in particular how are the time scales for the melting of the briquettes determined ?

- For both the experiment and full-sized electrode production, under what circumstances will too much air remain in the final product ?

- For the manufacture of Persson and Bruff electrodes using briquette replenishment what are the requirements in terms of time or electrode length for proper outflow of briquettes ?

- Can a mathematical model be posed that allows detailed (probably computational) analysis of briquette melting for the Persson and Bruff electrodes ?

2 Two-phase flow modelling

We begin by setting up a two-phase flow framework that will allow us to examine both the experiment and full-sized electrodes. Although subsequent simplifications will be made, the two-phase equations will be posed in some generality in order that the assumptions involved in the modelling may be clearly understood. Labelling the air and paste phases 1 and 2 respectively, the general picture is of a network of pores which slowly fill with melting paste as the temperature increases and close as the paste is compressed. The three-dimensional equations of two-phase flow may then be written (see Drew & Wood (1985))

$$(\alpha_1\rho_1)_t + \nabla.(\alpha_1\rho_1\boldsymbol{u}_1) = 0 \tag{1}$$

$$(\alpha_2\rho_2)_t + \nabla.(\alpha_2\rho_2\boldsymbol{u}_2) = 0 \tag{2}$$

$$(\alpha_1\rho_1\boldsymbol{u}_1)_t + \nabla.(\alpha_1\rho_1\boldsymbol{u}_1\boldsymbol{u}_1) = \nabla.(\alpha_1(\boldsymbol{T}_1 + \boldsymbol{T}_1^{Re})) + \alpha_1\rho_1\boldsymbol{g} + \boldsymbol{M}_1 \tag{3}$$

$$(\alpha_2\rho_2\boldsymbol{u}_2)_t + \nabla.(\alpha_2\rho_2\boldsymbol{u}_2\boldsymbol{u}_2) = \nabla.(\alpha_2(\boldsymbol{T}_2 + \boldsymbol{T}_2^{Re})) + \alpha_2\rho_2\boldsymbol{g} + \boldsymbol{M}_2 \tag{4}$$

$$\begin{aligned}(\alpha_1\rho_1 e_1)_t + \nabla.(\alpha_1\rho_1\boldsymbol{u}_1 e_1) = \alpha_1\boldsymbol{T}_1 : \nabla\boldsymbol{u}_1 - <\chi_1 p_1\nabla.\boldsymbol{u}_1'> -\nabla.\alpha_1(\boldsymbol{q}_1 + \boldsymbol{q}_1^{Re}) + \\ \alpha_1\rho_1 r_1 + E_1 + \alpha_1 D_1\end{aligned} \tag{5}$$

$$\begin{aligned}(\alpha_2\rho_2 e_2)_t + \nabla.(\alpha_2\rho_2\boldsymbol{u}_2 e_2) = \alpha_2\boldsymbol{T}_2 : \nabla\boldsymbol{u}_2 - <\chi_2 p_2\nabla.\boldsymbol{u}_2'> -\nabla.\alpha_2(\boldsymbol{q}_2 + \boldsymbol{q}_2^{Re}) + \\ \alpha_2\rho_2 r_2 + E_2 + \alpha_2 D_2\end{aligned} \tag{6}$$

In these equations (in which it has been assumed that there is no interphase mass exchange) α represents volume fraction ($\alpha_1 + \alpha_2 = 1$), ρ and $\boldsymbol{u}$ denote density and velocity respectively and a prime indicates fluctuating quantities, whilst $\boldsymbol{T}$ and $\boldsymbol{T}^{Re}$ denote respectively the stress and Reynolds' stress. (Standard tensor notation has been used here so that $\boldsymbol{A} : \boldsymbol{B} = A_{ji}B_{ij}$.) The gravity vector is given by $\boldsymbol{g}$, $\boldsymbol{M}$ denotes interfacial momentum source, $\boldsymbol{q}$ and $\boldsymbol{q}^{Re}$ are respectively the energy and turbulent energy fluxes and $\chi_i(\boldsymbol{x})$ is the phase indicator function which takes the value 1 if $\boldsymbol{x}$ is in phase i and zero otherwise. The terms E_k and D_k are respectively the interfacial heat source in phase k and the dissipation in phase k, whilst r denotes energy source terms. The pressure and internal energy are given by p and e respectively.

Is is important to note that the two-phase flow equations given above are posed entirely in terms of *ensemble averaged* variables. Although space does not permit a full discussion of such averaging procedures (which may be carried out in many different ways), we generally define the ensemble average $< f >$ of a field $f(\boldsymbol{x}, t)$ by

$$< f > = \int_M f(\boldsymbol{x}, t; \xi) dm(\xi)$$

where $m(\xi)$ is the probability of observing process ξ and M is the set of all such processes. The details of the averaging need not concern us, but it is worth remembering that the variables in the equations (1)-(6) have complicated definitions. For example, $\alpha_k = < \chi_k >$,

$\rho_k =< \chi_k\rho > / < \alpha_k >$ and $\boldsymbol{u}_k =< \chi_k\rho\boldsymbol{u} > /(< \alpha_k >< \rho_k >)$. It is therefore dangerous to interpret the averaged variables in a pointwise manner so that, for example, if it transpired that $\boldsymbol{u}$ was less than zero this does not mean that all the air particles have a positive velocity.

It is now necessary to invoke closure assumptions to derive a closed model from (1)-(6). In the momentum equations, we assume that the Reynolds' stress terms are negligible, the gravity vector is given by $\boldsymbol{g} = -g\boldsymbol{k}$ and that

$$\boldsymbol{T}_k = -p_k\delta_{ij} + \tau_k \qquad (\tau_k = \mu_k(\nabla\boldsymbol{u} + \nabla\boldsymbol{u}^T)),$$

where μ_k denotes the dynamic viscosity of phase k. The terms $\boldsymbol{M}_k$ represent the interfacial forces arising from stresses on the interface. It has become normal (see, for example Drew (1983)) to write

$$\boldsymbol{M}_k = p_{ki}\nabla\alpha_k + \boldsymbol{M}'_k \qquad (k = 1, 2)$$

where p_{ki} is the interfacially averaged pressure of phase k and the terms $\boldsymbol{M}'_k$ contain all forces that are related to drag, virtual mass and any other unsteady flow effects that might be important. Ignoring all such effects except for the interphase drag $\boldsymbol{D}_{ij}$ exerted on phase i due to phase j, we find that the momentum equations become

$$(\alpha_k\rho_k\boldsymbol{u}_k)_t + \nabla.(\alpha_k\rho_k\boldsymbol{u}_k\boldsymbol{u}_k) + \alpha_k\nabla p_k = \nabla.(\alpha_k\boldsymbol{\tau}_k) - \alpha_k\rho_k g\boldsymbol{k} +$$

$$(p_{ki} - p_k)\nabla\alpha_k + \boldsymbol{D}_{kj}$$

and it now only remains to deal with the energy equations. Much modelling and discussion is required here if the job is to be done carefully, but we adopt a simple approach, assuming that the interfacial heat sources and the dissipation are both zero. (Both of these assumptions may have to be reviewed in some circumstances, since the chemical reactions that bake the paste may provide extra heat sources and the viscous dissipation may be non-negligible under some circumstances. Extra heat transfer terms would also probably have to be included to ensure that the gas temperature was accurately predicted.) Assuming that fluctuation terms may be ignored, neglecting bulk energy sources and using the Fourier law $\boldsymbol{q}_k = -k_k\nabla T$ where T is temperature (as distinct from the tensor quantity $\boldsymbol{T}$) and k_k is the thermal conductivity of phase k, we find, using $e_k = c_{pk}T_k$ where c_p denotes the specific heat at constant pressure, that the three-dimensional two-phase flow equations may be written

$$(\alpha_1\rho_1)_t + \nabla.(\alpha_1\rho_1\boldsymbol{u}_1) = 0 \tag{7}$$

$$(\alpha_2\rho_2)_t + \nabla.(\alpha_2\rho_2\boldsymbol{u}_2) = 0 \tag{8}$$

$$(\alpha_1\rho_1\boldsymbol{u}_1)_t + \nabla.(\alpha_1\rho_1\boldsymbol{u}_1\boldsymbol{u}_1) + \alpha_1\nabla p_1 = \nabla.(\alpha_1\mu_1(\nabla\boldsymbol{u}_1 + (\nabla\boldsymbol{u}_1)^T)) +$$
$$-\alpha_1\rho_1 g\boldsymbol{k} + (p_{1i} - p_1)\nabla\alpha_1 + \boldsymbol{D}_{12} \tag{9}$$

$$(\alpha_2\rho_2\boldsymbol{u}_2)_t + \nabla.(\alpha_2\rho_2\boldsymbol{u}_2\boldsymbol{u}_2) + \alpha_2\nabla p_2 = \nabla.(\alpha_2\mu_2(\nabla\boldsymbol{u}_2 + (\nabla\boldsymbol{u}_2)^T)) +$$
$$-\alpha_2\rho_2 g\boldsymbol{k} + (p_{2i} - p_2)\nabla\alpha_2 + \boldsymbol{D}_{21} \tag{10}$$

$$(\alpha_1\rho_1 c_{p1}T_1)_t + \nabla.(\alpha_1\rho_1\boldsymbol{u}_1 c_{p1}T_1) = \alpha_1\boldsymbol{T}_1 : \nabla\boldsymbol{u}_1 + \nabla.(\alpha_1 k_1\nabla T_1) \tag{11}$$

$$(\alpha_2\rho_2 c_{p2}T_2)_t + \nabla.(\alpha_2\rho_2\boldsymbol{u}_2 c_{p2}T_2) = \alpha_2\boldsymbol{T}_2 : \nabla\boldsymbol{u}_2 + \nabla.(\alpha_2 k_2\nabla T_2) \tag{12}$$

The equations (7)-(12) may be thought of as the basic two-phase flow model, and may now be further simplified using some dimensional analysis. Scaling pressures with $\mu_2 U_2/L_2$ and time with L_2/U_2 where U_2 and L_2 are a typical speed and length scale in the paste flow, we find that, in the equation for the paste momentum, the ratio of inertial to viscous forces is given by

$$Re_2 = \frac{\rho_2 U_2 L_2}{\mu_2}.$$

Reasonable values for these parameters seem to be $\rho_2 \sim 1570$ kg/m^3, $U_2 \sim 1$cm/hour and $L_2 \sim 5$ cm, so that even when a paste viscosity value of $\mu_2 \sim 10^4$ (almost certainly a gross underestimate - see later discussion on paste viscosity) is assumed, we find that

$$Re_2 \sim 2 \times 10^{-8}.$$

Evidently under normal circumstances the viscous and the pressure terms in the equation must be retained, and since the ratio of gravity to viscous forces is given by

$$\frac{\text{gravity}_2}{\text{viscosity}_2} \sim \frac{\rho_2 g L_2^2}{\mu_2 U_2} \sim 10^7/\mu_2$$

and μ_2 ranges in order of magnitude from 10^4 to 10^8, the gravity term cannot normally be neglected. As far as the interfacial pressure term (which assumes such importance in many two phase flows) is concerned, we note that it seems likely that the bulk and interfacial pressures will be almost identical in both phases. This term is thus ignored. In the gas momentum equation, the ratios of inertial to pressure force and pressure to viscous forces are given by

$$\frac{\text{inertia}_1}{\text{pressure}_1} \sim \frac{U_2^2 u_1 \rho_1}{L_2 \mu_2} \sim \frac{10^{-2} u_1}{5\mu_2}$$

$$\frac{\text{pressure}_1}{\text{viscous}_1} \sim \frac{\mu_2 U_2}{\mu_1 U_1} \sim \frac{10\mu_2}{36 U_1}.$$

Inertia is therefore negligible also in the gas momentum equation, and the pressure forces are many orders of magnitude larger than the viscous forces, largely as a result of the very small value of the viscosity ratio μ_1/μ_2. Surface tension is also ignored in both equations as a simple order-of-magnitude argument suggests that it will play a non-trivial role only when the pore radius is less than about 10 μm. Ignoring the interfacial pressure term in the gas equation, assuming that both phases are incompressible and writing for simplicity $\alpha_2 = \alpha$, $\alpha_1 = 1 - \alpha$, we find that the two-phase flow equations reduce to

$$\alpha_t + \boldsymbol{\nabla}.(\alpha \boldsymbol{u}_2) = 0, \tag{13}$$

$$-\alpha_t + \boldsymbol{\nabla}.\left((1-\alpha)\boldsymbol{u}_1\right) = 0, \tag{14}$$

$$\alpha \boldsymbol{\nabla} p_2 = \boldsymbol{\nabla}.\left(\alpha\mu_2\left[\boldsymbol{\nabla}\boldsymbol{u}_2 + (\boldsymbol{\nabla}\boldsymbol{u}_2)^T\right]\right) - \rho_2 \alpha g \boldsymbol{k} + \boldsymbol{D}, \tag{15}$$

$$(1-\alpha)\boldsymbol{\nabla} p_1 = -\boldsymbol{D}. \tag{16}$$

The equations (13)-(16) will form the basis of our models for both the Elkem experiment and models of real electrodes. It will be noted that in these equations no consideration has been given to energy conservation. The modelling required to do this is made complicated by the terms $\alpha_k \boldsymbol{T}_k : \nabla \boldsymbol{u}_k$ ($k = 1, 2$, since for two phase flow the pressure term involved does not vanish. For the present we ignore this problem (work is currently in progress regarding this matter, but the term represents viscous dissipation and is almost certainly negligible under most circumstances) and use, when required, a simple one-phase temperature equation. It is also clear that the system (13)-(16) is not closed as it involves more unknowns than there are equations. To close the system we need a constitutive relation for the interactive drag $\boldsymbol{D}$, and a relation between p_1 and p_2. We make the simplifying assumption $p_1 = p_2$, and for $\boldsymbol{D}$ we observe the following scalings. If

$$\boldsymbol{u}_2 \sim U_2, \quad \boldsymbol{x} \sim L_2, \quad \text{say,}$$

then

$$\boldsymbol{u}_1 \sim \frac{\alpha U_2}{1-\alpha}, \quad p_{1,2} \sim \frac{\mu_2 U_2}{L_2},$$

and assuming Poiseuille/Stokes drag,

$$\boldsymbol{D} \sim \frac{\alpha \mu_1 \boldsymbol{u_1}}{R^2},$$

where R is a typical pore radius. Hence, after nondimensionalisation (16) reads

$$\boldsymbol{\nabla} p_1 \sim \frac{\mu_1}{\mu_2} \cdot \frac{L_2^2}{R^2} \cdot \frac{\alpha^2}{(1-\alpha)^2}. \tag{17}$$

Since $\mu_1/\mu_2 < O(10^{-10})$, we can take

$$p_1 = \text{const.} \tag{18}$$

at least until the pores shrink to the point that $R(1-\alpha)/L_2 \sim 10^{-5}$. Hence in this regime, (hereafter referred to as "**Regime I**") we obtain a closed system for α and $\boldsymbol{u}_2$ in the form

$$\alpha_t + \boldsymbol{\nabla}.(\alpha \boldsymbol{u}_2) = 0, \tag{19}$$

$$\nabla.\left(\alpha\mu_2\left[\boldsymbol{\nabla}\boldsymbol{u}_2 + (\boldsymbol{\nabla}\boldsymbol{u}_2)^T\right]\right) = \rho_2 \alpha g \boldsymbol{k}. \tag{20}$$

The above model may not hold for all stages of the process since it allows α to increase indefinitely. In practice, when α reaches some critical value, α_c say, the pores close off to form isolated packets or bubbles of air. Once this has occurred, α cannot change since the air is unable to escape, and the problem reduces to

$$\alpha = \alpha_c, \tag{21}$$

$$\boldsymbol{\nabla}.\boldsymbol{u}_2 = 0, \tag{22}$$

$$\boldsymbol{\nabla} p_2 = \alpha_c \boldsymbol{\nabla}.\left(\mu_2\left[\boldsymbol{\nabla}\boldsymbol{u}_2 + (\boldsymbol{\nabla}\boldsymbol{u}_2)^T\right]\right) - \rho_2 \alpha_c g \boldsymbol{k}. \tag{23}$$

We denote this regime by **Regime II**.

The transition between regimes I and II is complicated and unlikely to be easy to analyse. We therefore neglect the details of the transition and simply assert that Regime I applies whenever $\alpha < \alpha_c$, switching to Regime II for values of α that exceed α_c.

3 Analysis of the experiment

In the Elkem experiment, a cylinder of radius a (= 8.5 cm) is filled with paste briquettes, with an initial void fraction $(1 - \alpha_0)$, up to an initial height L (= 30 cm). A mass M is then loaded onto the top of the piston and the cylinder is heated to 100°C. As air is forced out by the weight of the loaded piston and of the paste itself, the mass moves downwards. Its position is plotted against time, and from this the average density of the air/paste mixture is deduced. It is observed that the density calculated by this method asymptotes to around 1430 kg/m^3, whereas the density of raw paste at such temperatures is about 1570 kg/m^3. The final density is thus about 91% of that of pure paste; this corresponds to α_c referred to earlier and we shall thus take $\alpha_c = 0.91$ in all numerical results given below. It might be argued that 'predictions' of the experimental data should not use this result as it comes itself from the experiment: however it is a parameter that is likely to be a property of the paste itself rather than the experiment. We therefore regard α_c as a 'known paste property'.

3.1 One dimensional model

We model the flow in the experiment as one-dimensional, with the fluid velocity $\boldsymbol{u}_2 = w(z,t)\boldsymbol{k}$. We first consider the simple case in which the paste has constant viscosity μ_2, though later we allow for temperature-dependent viscosity. We nondimensionalise using

$$z = L\tilde{z}, \quad s = L\tilde{s}, \quad w = \frac{MgL}{2\pi a^2 \mu_2}\tilde{w}, \quad t = \frac{2\pi a^2 \mu_2}{Mg}\tilde{t}, \tag{24}$$

where the moving top of the experiment (i.e. the bottom surface of the piston) is denoted by $z = s(t)$. The equations (19, 20) become (dropping tildes)

$$\alpha_t + (\alpha w)_z = 0, \quad (\alpha w_z)_z = g^* \alpha. \tag{25}$$

Here

$$g^* = \frac{\pi a^2 \rho_2 L}{M} \tag{26}$$

measures the relative importance of the weight of the briquettes themselves compared to that of M.

The origin for z is chosen to be the bottom of the cylinder. The boundary conditions for (25) are that the void fraction is specified at $t = 0$ when the moving top of the experiment is at $s = 1$. We must also have $w = 0$ on $z = 0$. To determine the unknown boundary $s(t)$ evidently we must have $w = \dot{s}$ when $z = s$. In addition to this, the load is known. Since the effect of the load is communicated to the briquette column by the briquettes themselves, the (dimensional) pressure on the moving top is

$$-\frac{Mg}{\alpha \pi a^2}.$$

This must equal $2\mu_2 w_z$, and the final (non-dimensional) boundary conditions thus become

$$\begin{array}{lll} \alpha = \alpha_0, & & t = 0, \\ w = 0, & & z = 0, \\ \alpha w_z = -1, & w = \dot{s}, & z = s \\ s = 1, & & t = 0. \end{array} \tag{27}$$

The unsteady, nonlinear free boundary problem (25, 27) may be solved explicitly, (there are many ways to do this, but transforming to Lagrangian variables is probably the simplest) giving

$$\begin{aligned} \alpha &= \left[\alpha_0(1+g^*t)+t\right] e^{-g^*zt}, \\ w &= \frac{\alpha_0\left(e^{g^*zt}-1\right)}{g^*t^2\left[\alpha_0(1+g^*t)+t\right]} - \frac{z}{t}, \\ s &= \frac{1}{g^*t}\log\left(\frac{\alpha_0(1+g^*t)+t}{\alpha_0+t}\right). \end{aligned} \tag{28}$$

As noted in section 2 this solution must eventually become invalid. (For example, when $z=0$ the void fraction α increases indefinitely.) Hence there is a shift to regime II when α reaches α_c, which occurs first at $z=0, t=t_c$, where

$$t_c = \frac{\alpha_c-\alpha_0}{1+\alpha_0 g^*}.$$

For $t > t_c$ we introduce a second free boundary $z = l(t)$ such that we have Regime I in $z > l$ and Regime II in $z < l$. The new free boundary problem that results is (25, 27) in $l < z \leq s$, with the additional boundary conditions

$$\begin{aligned} &\alpha = \alpha_c, w = 0 \quad && z = l, \\ &l = 0 && t = t_c. \end{aligned} \tag{29}$$

This problem may also be solved in closed form, giving

$$\begin{aligned} \alpha &= \alpha_c \exp\left(\frac{\alpha_0-\alpha_c+(1+\alpha_0 g^*)t-\alpha_c g^* zt}{\alpha_c}\right), \\ w &= \frac{1+\alpha_0 g^*}{\alpha_c g^* t} - \frac{1}{g^*t^2} - \frac{z}{t} + \frac{\alpha_0}{\alpha_c g^* t^2}\exp\left(\frac{\alpha_c-\alpha_0-(1+\alpha_0 g^*)t+\alpha_c g^* zt}{\alpha_c}\right), \\ s &= \frac{1+\alpha_0 g^*}{\alpha_c g^*} - \frac{\alpha_c-\alpha_0}{\alpha_c g^* t} + \frac{1}{g^*t}\log\left(\frac{\alpha_c}{\alpha_0+t}\right), \\ l &= \frac{(1+\alpha_0 g^*)(t-t_c)}{\alpha_c g^* t}. \end{aligned} \tag{30}$$

Notice that after time $t = \alpha_c - \alpha_0$, we have $s = l$. At this point $\alpha = \alpha_c$ everywhere and the process stops.

In figure 2 α is plotted against z for increasing values of t using the parameters $g^* = 2$, $\alpha_0 = 0.45$ and $\alpha_c = 0.91$. With these values $t_c = 0.242$, and indeed for $t > 0.242$ we observe a region near $z = 0$ in which $\alpha = \alpha_c$. The process stops with $\alpha \equiv \alpha_c$ everywhere after time $\alpha_c - \alpha_0 = 0.46$. The two free boundaries $s(t)$ and $l(t)$ are plotted against t in figure 3 for the same parameter regime.

For the experiment g^* is actually about 0.34. Physically this means that the mass M is about three times heavier than the paste itself. We plot α against z in figure 4, and s and l against t in figure 5 for this parameter regime. With g^* small, α stays nearly spatially uniform as t increases. Hence, $t_c = 0.399$ and the final time $\alpha_c - \alpha_0 = 0.46$ are nearly equal, and so the free boundary l rises very rapidly to meet s. This suggests that a reasonable approximation may be obtained by setting $g^* = 0$, which simplifies the problem considerably since we can then neglect $l(t)$ completely.

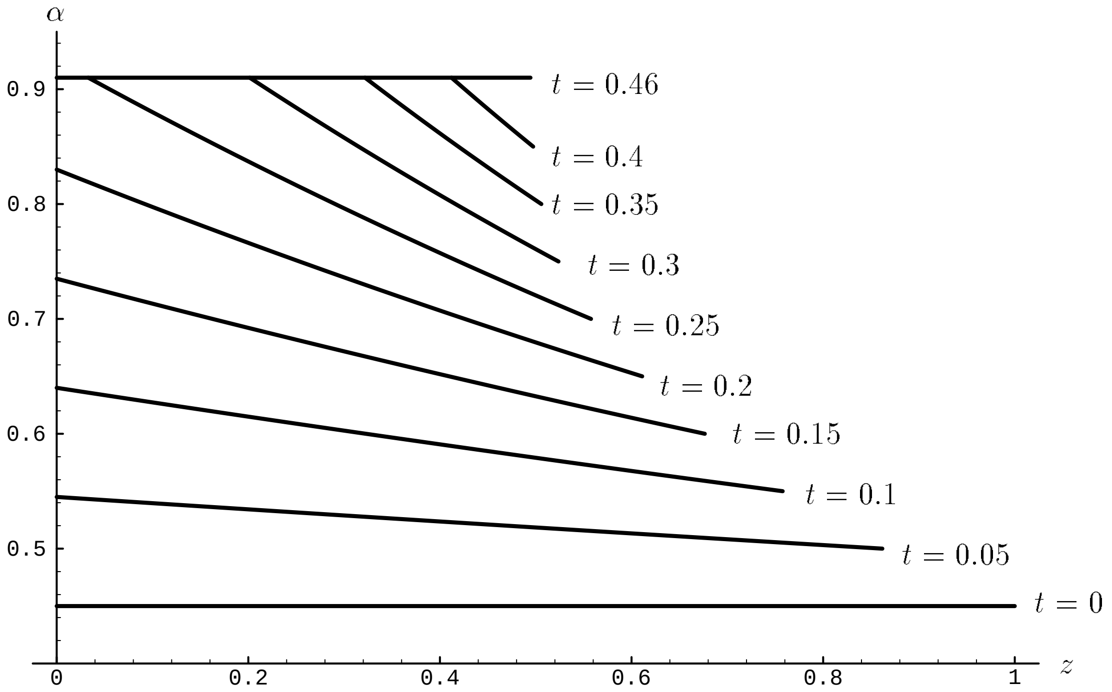

Figure 2: Paste volume fraction α versus height z for increasing values of time t. Here $g^* = 2$, $\alpha_0 = 0.45$, $\alpha_c = 0.91$.

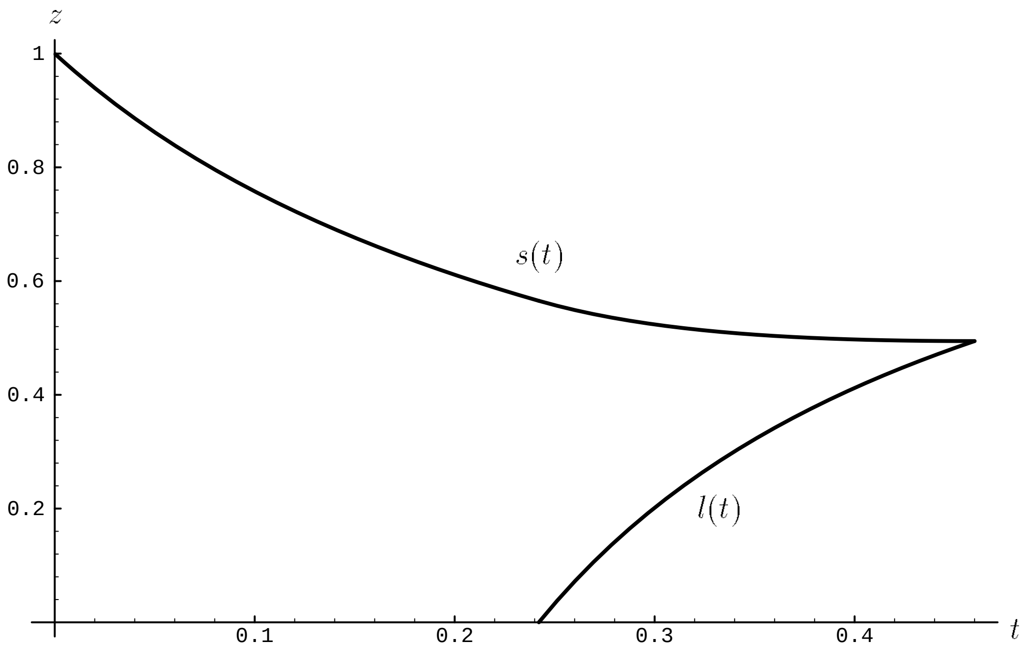

Figure 3: Free boundaries $z = s(t)$ and $z = l(t)$ versus time t. Here $g^* = 2$, $\alpha_0 = 0.45$, $\alpha_c = 0.91$.

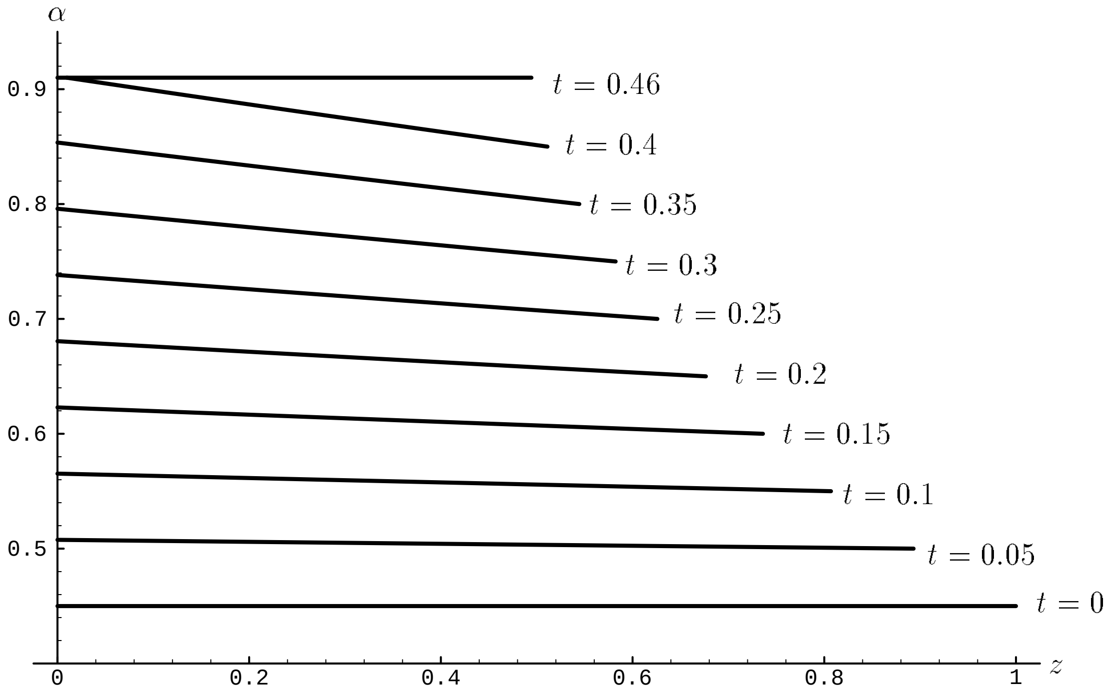

Figure 4: Paste volume fraction α versus height z for increasing values of time t. Here $g^* = 0.34$, $\alpha_0 = 0.45$, $\alpha_c = 0.91$.

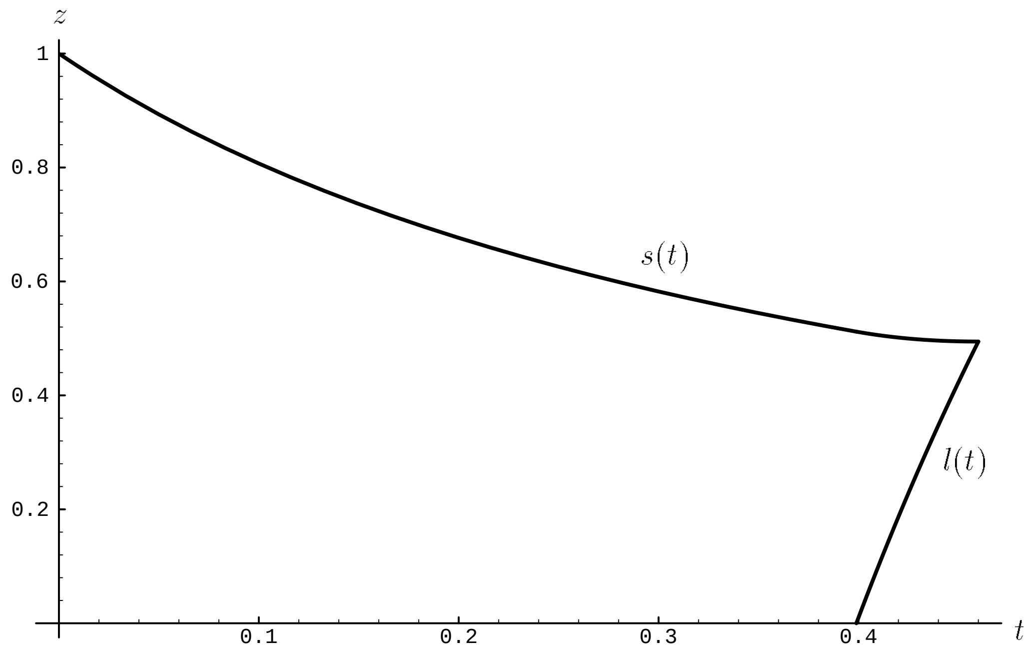

Figure 5: Free boundaries $z = s(t)$ and $z = l(t)$ versus time t. Here $g^* = 0.34$, $\alpha_0 = 0.45$, $\alpha_c = 0.91$.

3.1.1 Variable viscosity

The analysis carried out thus far may be expected to apply to the final stages of the experiment, when the temperature, and hence the viscosity, of the paste has become uniform. Alternatively, it may be regarded as relevant to an experiment where the briquettes are 'preheated' to the furnace temperature before they are squashed by the piston. If the Elkem experiment is to be properly simulated, however, then account must be taken of initial stages, where changes in viscosity of the slowly heated paste become important. We assume that the cylinder is heated uniformly and insulated at its top and bottom. This means that the temperature should be independent of z. Averaging across the cross-section to obtain a one-dimensional model as before, we obtain (in dimensional variables)

$$\alpha_t + (\alpha w)_z = 0, \quad 2\bar{\mu}_2(\alpha w_z)_z = \rho_2 \alpha g, \tag{31}$$

where $\bar{\mu}_2$, the cross-sectional average of the paste viscosity μ_2, is a function only of t. The dimensional boundary conditions are

$$\begin{array}{ll} \alpha = \alpha_0, & t = 0, \\ w = 0, & z = 0, \\ 2\bar{\mu}_2(t)\alpha w_z = -\frac{Mg}{\pi a^2}, \quad w = \dot{s}, & z = s \\ s = L, & t = 0. \end{array} \tag{32}$$

Motivated by our earlier observation that the gravity term in the momentum equation is rather small, we neglect the right hand side of the second equation of (31) for simplicity. Then the solution of (31) with boundary conditions (32) is simply

$$\alpha = \alpha_0 + F(t), \quad w = -\frac{\dot{F}z}{\alpha_0 + F}, \quad s = \frac{L\alpha_0}{\alpha_0 + F(t)} \tag{33}$$

where

$$F(t) = \int_0^t \frac{Mg}{2\pi a^2 \bar{\mu}_2(t')} dt'. \tag{34}$$

As noted earlier, now that gravity has been neglected in the momentum equation, α remains spatially uniform. Thus when α reaches α_c, it does so over the whole cylinder simultaneously. This simplifies matters greatly as a second free boundary does not have to be introduced.

Although (33) provides a simple expression for s (we have not included it in our comparisons below, but it would be easy to compute) it is actually not too hard to solve the equations when the gravity term is included, thus providing another case for comparison. We first solve (31) with boundary conditions (32) to yield

$$\begin{aligned} \alpha &= (\alpha_0 + (1 + \alpha_0 g^*)F) \exp\left(-\frac{g^* F z}{L}\right) \\ w &= \frac{L\alpha_0 \dot{F}(\exp(g^* F z/L) - 1)}{g^* F^2(\alpha_0 + (1 + g^*\alpha_0)F)} - \frac{\dot{F}z}{F} \\ s &= \frac{L}{g^* F} \log\left(\frac{\alpha_0 + (1 + g^*\alpha_0)F}{\alpha_0 + F}\right) \end{aligned} \tag{35}$$

where now

$$F(t) = \frac{Lg\rho_2}{2g^*} \int_0^t \frac{dt'}{\bar{\mu}_2(t')}$$

and g^* is as defined previously in (26). This solution is valid only until α reaches α_c, which happens first at $z = 0$, $t = t_c$ where

$$F(t_c) = \frac{\alpha_c - \alpha_0}{1 + \alpha_0 g^*}.$$

For $t > t_c$ we need to introduce another free boundary and solve (31) in the region $l(t) < z < s(t)$ with the boundary conditions

$$\begin{array}{ll} \alpha = \alpha_c, & z = l(t), \\ w = 0, & z = l(t), \\ 2\bar{\mu}_2(t)\alpha w_z = -\frac{Mg}{\pi a^2}, \quad w = \dot{s}, & z = s \\ l = 0, & t = t_c. \end{array}$$

The solution is given by

$$\begin{aligned} \alpha &= \alpha_c \exp\left(\frac{(1 + g^*\alpha_0)F + \alpha_0 - \alpha_c}{\alpha_c} - \frac{g^* F z}{L}\right) \\ w &= \frac{L\dot{F}}{g^* F^2}\left(\log\left(\frac{\alpha}{\alpha_c}\right) + \alpha_0\left(\frac{1}{\alpha} - \frac{1}{\alpha_c}\right)\right) \\ s &= \frac{L}{g^*\alpha_c}\left(1 + g^*\alpha_0 - \frac{\alpha_c - \alpha_0}{F} + \frac{\alpha_c}{F}\log\left(\frac{\alpha_c}{\alpha_0 + F}\right)\right) \\ l &= \frac{L}{g^*\alpha_c}\left(1 + g^*\alpha_0 - \frac{\alpha_c - \alpha_0}{F}\right). \end{aligned} \tag{36}$$

The whole process stops with $\alpha - \alpha_c$ and $w = 0$ everywhere when $t = t_f$ where

$$F(t_f) = \alpha_c - \alpha_0.$$

To make realistic comparisons with experimental data, all that remains to be determined is $\bar{\mu}_2(t)$. To do this we must consider the heat flow into the cylinder.

3.2 Heat flow

The transfer of heat into the paste during the experiment can be modelled using the cylindrically-symmetric heat equation. Normally this will give rise to a convection-diffusion equation that must be solved numerically. Under the assumptions that the cylinder is heated uniformly and insulated at its top and bottom so that the temperature is independent of z, whilst the flow is one-dimensional so that $u = 0$, however, the problem may be solved in closed form. We have (though see later remarks concerning the validity of this equation)

$$\rho_2 c \frac{\partial T}{\partial t} = k\left(\frac{\partial^2 T}{\partial r^2} + \frac{1}{r}\frac{\partial T}{\partial r}\right), \tag{37}$$

with the boundary conditions (see later discussion)

$$T = T_0 \text{ at } t = 0, \quad T = T_1 \text{ on } r = a. \tag{38}$$

In the experiment, the diameter of the cylinder is 17cm and thus $a = 8.5$cm. Taking T_0 to be room temperature (say 20°C) and T_1 as the furnace temperature 100°C, We nondimensionalise as follows:

$$r = a\tilde{r}, \quad t = \frac{\rho_2 c a^2}{k}\tilde{t}, \quad T = T_1 + (T_0 - T_1)\tilde{T}, \tag{39}$$

so that the problem becomes, on dropping the tildes,

$$T_t = T_{rr} + \frac{T_r}{r}, \quad T = 1 \text{ at } t = 0, \quad T = 0 \text{ on } r = 1. \tag{40}$$

The thermal conductivity and specific heat of raw paste are $k = 2.5$W/m/K and $c_p =$ 900J/kg/K respectively. Using a raw paste density of 1570 kg/m^3, the time scale implied by (39) is thus about 1.1 hours. We note first that this seems well in line with the experimental results and second that it is not possible to further simplify by making the heat-flow problem quasi-steady.

The solution of (40) is

$$T = \sum_{k=0}^{\infty} \frac{2J_0(rp_k)e^{-p_k^2 t}}{p_k J_1(p_k)}, \tag{41}$$

where p_k ($k = 0, 1, 2.....$) are the zeroes of J_0. These are given by $p_0 \sim 2.405$, $p_1 \sim 5.520$, $p_2 \sim 8.654$ and, for large k,

$$p_k \sim \pi(k + 3/4) + o(1),$$

an approximation that gives remarkably good results even for modest values of k. (Two decimal place accuracy is obtained even when $k = 0$.) The temperature may now be averaged across a cross-section, giving

$$< T >= 2\int_0^1 Tr\,dr = \sum_{k=0}^{\infty} \frac{4e^{-p_k^2 t}}{p_k^2}. \tag{42}$$

so that in dimensional variables

$$< T >= T_1 + (T_0 - T_1)\sum_{k=0}^{\infty} \frac{4}{p_k^2} \exp\left(-\frac{p_k^2 k t}{\rho_2 c a^2}\right) \tag{43}$$

Now that the temperature has been determined, we must give some thought to the viscosity that will be used to predict the experimental results. Paste viscosity was measured for a range of thermal conditions by Tørklep (1988). Using his results and after discussion with Elkem, it seems that a good approximation for paste viscosity between 50 and 150°C is given by an Arrhenius type law. An extra complication arises as to the exact nature of the constants appearing in the Arrhenius law, for the viscosity of the paste used in the Elkem experiment is at present classified. All that may be assumed is that the paste has a viscosity of 10^4 Pa s at 150°C and is 'similar to anode paste but less temperature dependent'. In normal circumstances the viscosity of paste depends quite strongly on the amount of coke contained in the paste, but using the given (incomplete) data in conjunction with Tørkelp's results, we propose a paste viscosity law given by

$$\mu_2 = 6.31 \times 10^{-20} \exp\left(\frac{22597}{T}\right) \tag{44}$$

where μ_2 is given in Pa s and the temperature in Kelvin. This formula assumes that the viscosity at 75°C is 10^9 Pa s and thus predicts a viscosity of 1.288×10^7 at the experimental steady state temperature of 100°C as well as a viscosity of 10^4Pa s at 150°C. Obviously this formula should be treated with caution and updated when fuller details of the paste viscosity are known. It is also worth noting that the size of the exponent in (44) means that a high activation energy asymptotic approach will almost certainly lead to some simplifications: this is not pursued further here.

3.3 Comparisons with experimental results

In order to compare with the tests performed at Elkem, the height of the piston during the experiment must be related to the effective density of the paste/air mixture. Defining the mixture density ρ_m by

$$\rho_m = \alpha\rho_2 + (1-\alpha)\rho_1 \tag{45}$$

we note that since the amount of paste in the experimental apparatus is conserved (unlike the air, which escapes during the experiment), we have, when the piston is at a height s,

$$\int_0^s \rho_2\alpha = C$$

where C is constant. Consideration of the conditions at the start of the experiment now shows that $C = L\rho_2\alpha_0$. Integrating (45) between 0 and s and assuming that ρ_m is constant in space then gives

$$\rho_m = \rho_1 + \frac{L\alpha_0}{s}(\rho_2 - \rho_1).$$

Since in the experiment being analysed ρ_1/ρ_2 is less than 10^{-3}, we simply use

$$\rho_m = \frac{L\alpha_0\rho_2}{s} \tag{46}$$

for comparison purposes.

Figure 6 shows comparisons between theoretical and experimental results. The symbols denote the results from two experiments, the density having been inferred from the position of the piston using (46). The broken line is plotted using the constant viscosity one-dimensional model, the viscosity at 100°C having been used. As expected, the rise is much too sharp in comparison with the experimental results. The solid line is plotted using (43), (35) and (36); the relevant values of t_c and t_f were 2586 and 2733 seconds respectively, showing that regime II persists for only a relatively short time in this case (a result consistent with the conclusions of figure 4). The inclusion of the slower rise in temperature gives results that are better in agreement with the experimental data, especially at the start of the process. For later times, however, agreement is poor. There are a number of possible reasons for this apart from the the uncertainty in the values of the viscosity mentioned above. These include

- The thermal conductivity of paste has been used. In the early stages of the process the experimental apparatus also contains some air, which has a much lower thermal conductivity. Averages should really be used for the thermal conductivity (and possibly other thermal variables as well).

- For simplicity it has been assumed that the temperature in the experiment is governed by (37). As noted in section 2, more consideration of the role of the pressure terms in the energy equation is required. Work on this is continuing at present.

- It is not absolutely clear how the experiment is begun. If the oven is switched on at the start of the process then presumably some heating time is required before a uniform temperature is reached. (Note added after Study Group: In fact the oven *is* switched on at the start of the process. The heating time is only a few minutes, however.)

- It may be unrealistic to assume that the ends of the experimental apparatus are thermally insulated.

- There is an inherent assumption in the model that although the temperature varies with r and not with z, the void fraction of paste varies with z but not with r. This is obviously unrealistic.

- Clearly it would be more realistic to replace the second boundary condition of (38) with a Newton heating boundary condition. For simplicity, this was not done during the Study Group, but the changes required would be easy to carry out. The only uncertainty would be in determining a realistic value for the heat transfer coefficient.

We conclude that although the model is producing very encouraging results (the sensitivity of (44) suggests that even to obtain order of magnitude agreement is a non-trivial achievement) more work is needed. This is continuing at present.

4 The Persson Electrode

4.1 The full problem

Elkem were keen that at some point during our consideration of this problem, a full model was posed to model the paste flow and baking in the Persson electrode. Figure 7 show that different regions that must be considered. For simplicity cartesian coordinates have been used; the real electrodes are cylindrical.

The full model of the Persson electrode may be written as follows:

'Bricks and flow' region:

$$\alpha_t + \operatorname{div}(\alpha \boldsymbol{q}) = 0$$

$$\rho c(T_t + (\boldsymbol{q}.\nabla)T) = \nabla.(k\nabla T) + h \mid \nabla\phi \mid^2$$

$$\operatorname{div}(\alpha\mu\nabla\boldsymbol{q}) = \rho g \alpha \boldsymbol{k}$$

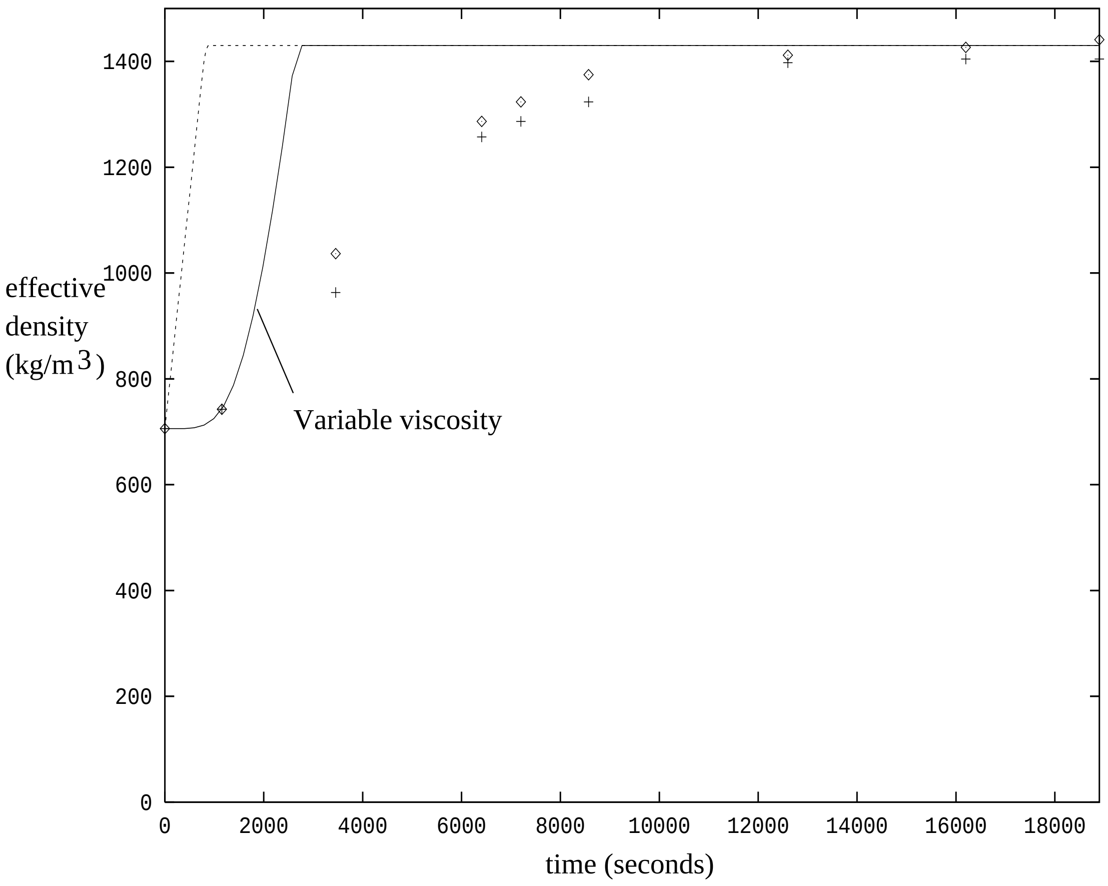

Figure 6: Comparison between theory and experimental data

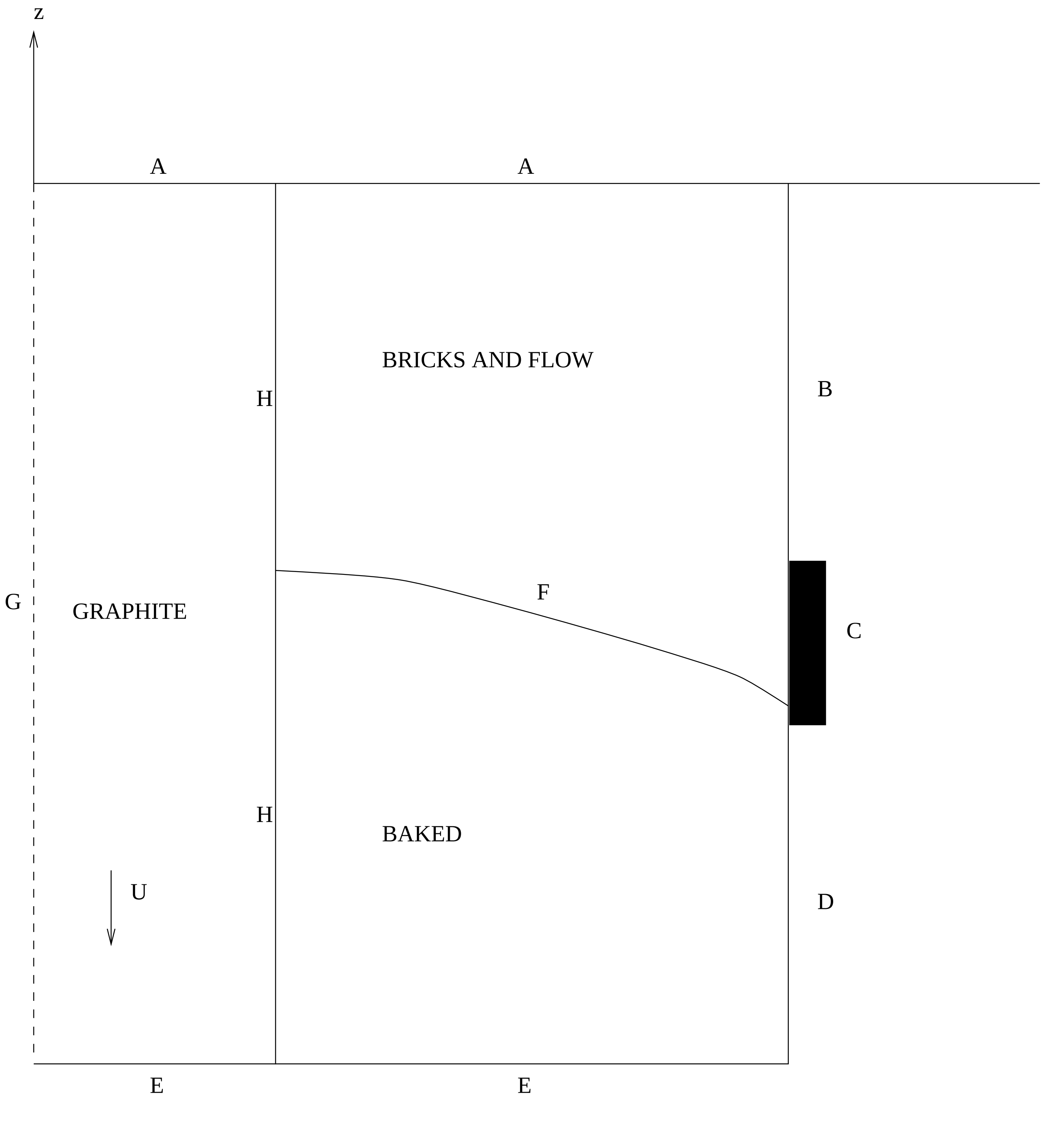

Figure 7: Model of paste flow and baking in Persson electrode

$$\mathrm{div}(\sigma\nabla\phi) = 0$$

'Baked' region:

$$\alpha = \alpha(x, S_B(x))$$

$$\rho c(T_t - UT_z) = \nabla.(k\nabla T) + h \mid \nabla\phi \mid^2$$

$$\boldsymbol{q} = -U\boldsymbol{k}$$

$$\nabla.(\sigma(\alpha, T)\nabla\phi) = 0$$

'Graphite' region:

$$\rho_G c_G(T_t - UT_z) = \nabla.(k_G\nabla T) + h \mid \nabla\phi \mid^2$$

$$\nabla.(\sigma_G(T)\nabla\phi) = 0$$

boundary A:	$T = T_A$ (given),	$\boldsymbol{q}_n = 0$,	$\alpha = \alpha_B(x,t)$ (given), $\phi_z = 0$.
boundary B:	$\boldsymbol{q} = 0$,	$\phi_x = 0$,	$T = T_{BL}(z)$ (given),
boundary C:	$\phi = 1$		
boundary D:	$\phi_x = 0$,	$T = T_f$ (given),	
boundary E:	$\phi = 0$,	$T = T_f$ (given),	
boundary F:	$T = T_B$ (given),	$[kT_n]_-^+ = 0$	
boundary G:	$T_x = 0$	$\phi_x = 0$	
boundary H:	$[T] = 0$,	$[T_x] = 0$.	

Here the subscript G refers to properties of the graphite, σ denotes electrical conductivity and ϕ the electric potential. The constant h is related to Joule heating (though in the bricks and flow region the conductivity is probably too small for Joule heating to be important). The latent heat of paste baking has been ignored. In its full form, this comprises an unsteady two-dimensional problem. Because of the simplifications made earlier, however, it is not nearly so formidable a problem to solve numerically as the full two phase/flow/heating problem that would results if the simplifications detailed above had not taken place. If Elkem wished to develop a sophisticated predictive tool for the analysis of Persson electrode paste melting and baking then it seems likely that a model similar to this could be used. For the present, however, we do not consider this full model further but content ourselves with analysing some simplified cases.

4.2 Time scales for air expulsion in the electrode

Using the models already developed it is clear how the time scales for paste melting and baking in the Persson electrode may be determined. The length scale L_C for pore closure is given essentially by a balance between gravity and viscosity, so that

$$L_C \sim \sqrt{\frac{\mu_2 U}{\rho_2 g}}.$$

Now simply using $t_C = L_C/U$ gives the pore closing time scale as

$$t_C \sim \sqrt{\frac{\mu_2}{\rho_2 g U}}.$$

If $U = 0.5\text{m/day} \approx 6 \cdot 10^{-6}$ m/s, $\rho_2 \approx 10^3$ kg/m^3 and $\mu_2 \approx 10^n$Pa s (because of uncertainties in the values of the viscosity as discussed previously we use an exponent n) then

$$L \sim 10^{n/2-5} m.$$

Hence so long as $\mu_2 < 10^{10}$ Pa s, (almost certainly the case in practice) all the air that is going to escape will do so within about 1 metre. This indicates that region II applies everywhere except in a small region near to the top of the electrode. This result is in stark contrast to the experiment where region I is normally the dominant one. One way of interpreting this result is to conclude that the experiment could be made 'more relevant' by increasing the value of g^*. Indeed, it is possible that 'scaling up' results of this sort may turn out to be the most important modelling conclusions from a practical point of view.

4.3 One-dimensional model

We use a one-dimensional approximation for the fluid mechanics in the electrode equivalent to that used to model the experiment in section 3.1. We nondimensionalise the vertical velocity component w with the electrode velocity $U = 0.5$ metres per day $\approx 6 \cdot 10^{-6}$ m s^{-1}, and vertical distance z with the characteristic length scale

$$L = \sqrt{\frac{2\mathcal{M}_2 U}{\rho_2 g}}, \tag{47}$$

where $\mathcal{M}_2$ is a typical value of the temperature-dependent paste viscosity μ_2.

We seek a steady state so that the equations of motion reduce to

$$\alpha w = -Q, \quad (\bar{\mu}_2 \alpha w_z)_z = \alpha, \tag{48}$$

where Q, the flux of paste, is a constant, as yet unknown. (Although we know the velocity at the bottom of the baked region, we do not know the void fraction of paste that will eventually be 'baked in'.) The initial conditions for this system are zero stress and given α at the top of the electrode $z = 0$:

$$\alpha(0) = \alpha_0, \quad w_z(0) = 0. \tag{49}$$

Finally, at the point, $z = -b$ say, where the paste becomes baked and therefore solid, it is then constrained to move with the imposed electrode speed U, and so

$$w(-b) = -1. \tag{50}$$

The three boundary conditions enable us in principle to solve the second-order o.d.e. (48b) and then to find the constant Q. To do so we need to know the functional form of $\bar{\mu}_2(z)$, which entails solving the coupled electrostatics and heat-transfer problems. Some insight into the behaviour to be expected is gained by considering the following simplified scenario. Suppose the briquettes remain solid at the top of the electrode until they reach a point $z = -m$ at which they melt. Thereafter they have constant viscosity until they reach the baking point $z = -b$, at which they become solid once more. The problem then reduces to

$$\begin{array}{lll} \alpha = -Q/w, \quad w(w_z/w)_z = 1, & & -b < z < -m, \\ w_z = -m, \quad \alpha = \alpha_0, & & z = -m, \\ w = -1, & & z = -b. \end{array} \tag{51}$$

Note that $l = b - m$ is the length of the melted zone. The form of the solution of (51) depends on the relative sizes of l and the length m of the unmelted zone. For $m > l + \sqrt{2}$,

$$w = -\frac{\sinh^2\left(D + \frac{(z+b)\sinh D}{\sqrt{2}}\right)}{\sinh^2 D}, \tag{52}$$

where the constant D is the unique positive solution of

$$\sinh\left(2D + \sqrt{2}l \sinh D\right) = \sqrt{2}m \sinh D. \tag{53}$$

For $0 \le m < l + \sqrt{2}$, the solution is

$$w = -\frac{\cos^2\left(D - \frac{(z+b)\cos D}{\sqrt{2}}\right)}{\cos^2 D}, \tag{54}$$

where D satisfies

$$\sin\left(2D - \sqrt{2}l \cos D\right) = \sqrt{2}m \cos D. \tag{55}$$

For the solution to be bounded, D must lie in the range $D^* \le D < \pi/2$, where D^* is the unique root in $[0, \pi/2]$ of

$$\sqrt{2}D^* \sec D^* = l, \tag{56}$$

and $D = D^*$ corresponds to $m = 0$. With D constrained to lie in $[D^*, \pi/2)$, (55) has a unique solution.

Finally, in the special case $m = l + \sqrt{2}$, the solution is simply

$$w = -\left(1 + \frac{(z+b)}{\sqrt{2}}\right)^2. \tag{57}$$

The main item of interest as far as the practical electrode production process is concerned is of course the "baked-in" volume fraction α_b which determines whether or not the briquette-produced electrode is of sufficient strength and electrical conductivity. This is given by

$$\frac{\alpha_b}{\alpha_0} = -w(-m). \tag{58}$$

We can eliminate D from this expression and so obtain a relation between α_b/α_0 and the two parameters l and m:

$$l = \frac{\cos^{-1}\sqrt{\frac{\alpha_0}{\alpha_b}\left(1 - \frac{m^2\alpha_0}{2\alpha_b}\right)} - \sin^{-1}\sqrt{\frac{m^2\alpha_0}{2\alpha_b}}}{\sqrt{\frac{\alpha_0}{2\alpha_b}\left(1 - \frac{m^2\alpha_0}{2\alpha_b}\right)}} \quad \text{for } m < \sqrt{\frac{2\alpha_b}{\alpha_0}}, \tag{59}$$

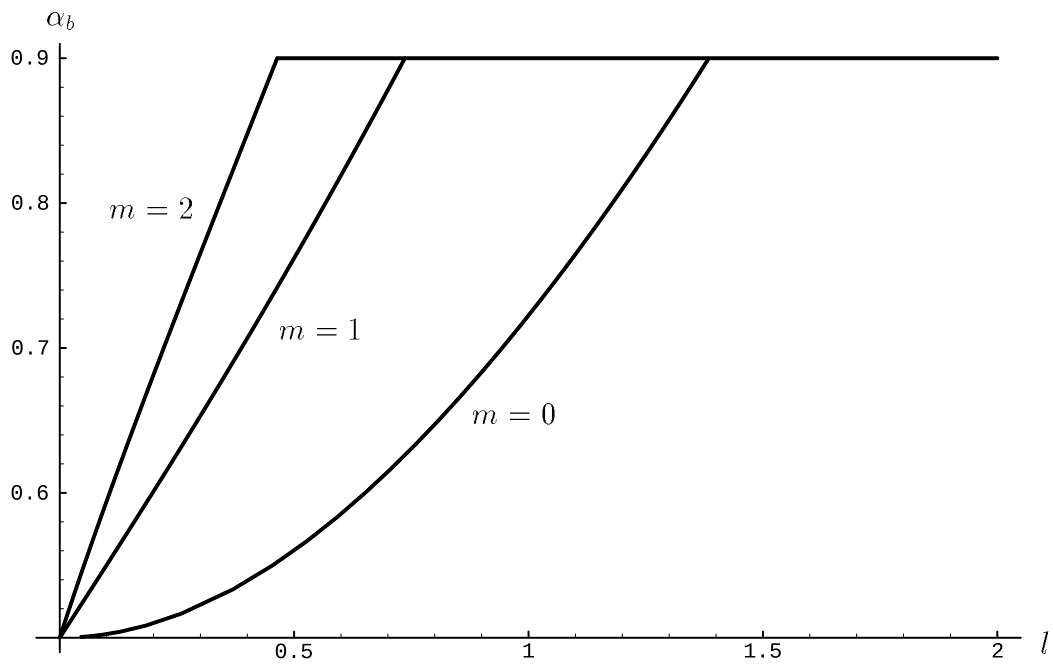

Figure 8: Baked-in paste volume fraction α_b versus length of the melted zone l, for various values of the length of the unmelted zone m. Here $\alpha_0 = 0.5$, $\alpha_c = 0.9$.

$$l = \frac{\cosh^{-1}\sqrt{\frac{m^2\alpha_0}{2\alpha_b}} - \sinh^{-1}\sqrt{\frac{\alpha_0}{\alpha_b}\left(\frac{m^2\alpha_0}{2\alpha_b} - 1\right)}}{\sqrt{\frac{\alpha_0}{2\alpha_b}\left(\frac{m^2\alpha_0}{2\alpha_b} - 1\right)}} \quad \text{for } m > \sqrt{\frac{2\alpha_b}{\alpha_0}}, \tag{60}$$

$$l = \sqrt{2}\left(\sqrt{\frac{\alpha_b}{\alpha_0}} - 1\right) \quad \text{for } m = \sqrt{\frac{2\alpha_b}{\alpha_0}}. \tag{61}$$

On physical grounds, we anticipate that the baked-in volume fraction α_b should be an increasing function of both m (which is effectively the weight pushing down on the melted zone) and the length of the melted zone l. However, the expressions (59–61) are only valid for $\alpha_b \leq \alpha_c$, where α_c is the maximum possible value of α defined earlier. If α reaches α_c at any point in the electrode (above the baking zone) then it remains at that value thereafter. We denote by l_c the critical value of l such that α_b first equals α_c at $l = l_c$. Then if l is increased past l_c, (59–61) cease to apply and α_b simply stays at the value α_c.

We plot α_b against l in figure 8, for various values of m, using the parameter values $\alpha_0 = 0.5$ and $\alpha_c = 0.9$. In order to maximise the strength of the baked electrode, it is desirable to make α_b as large as possible. In order to do so, one should ensure that $l > l_c$ so that α_b is at its maximum value of α_c. We plot l_c versus m in figure 9, for the same values of α_0 and α_c. The dotted line shows the transition between solutions (59) and (60).

Because of the gross simplifying assumptions made regarding the viscosity, the results of this simple model of the Persson electrode should be regarded as merely qualititative. Nevertheless, they provide some valuable insight into the process of manufacturing briquette-charged electrodes.

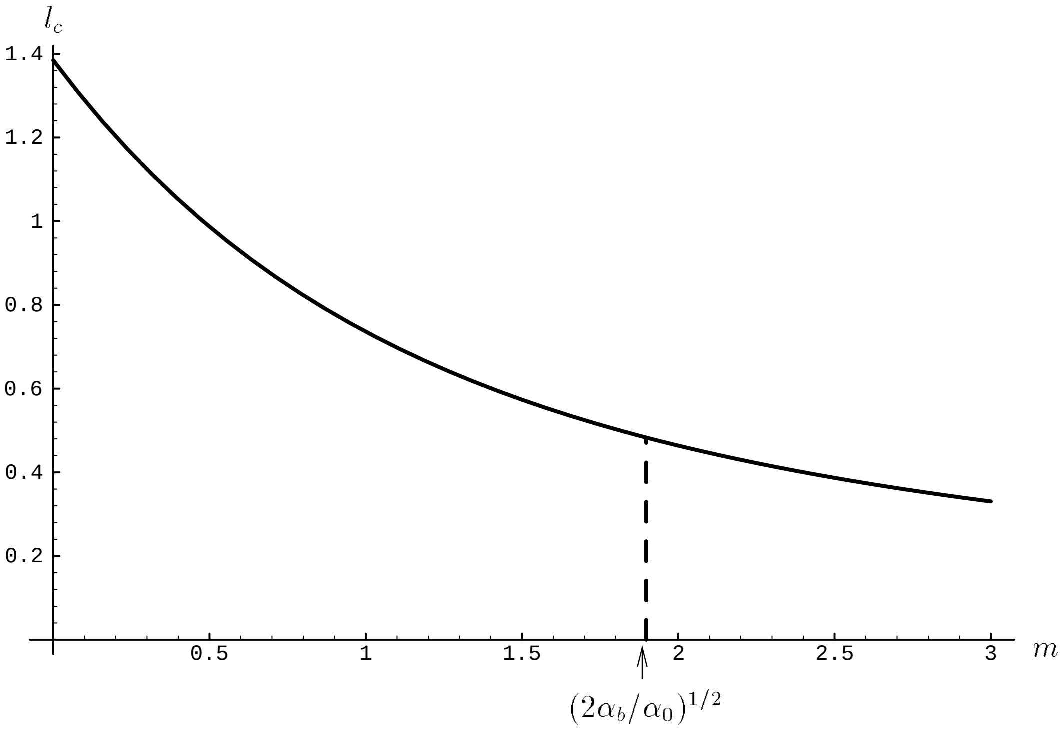

Figure 9: Critical length l_c of the melted zone, above which the maximum possible paste volume fraction is achieved, versus length m of the unmelted zone. Here $\alpha_0 = 0.5$, $\alpha_c = 0.9$. The dotted line shows point of transition between the two different solutions.

5 Conclusions and discussion

The work discussed above should be thought of as a record of the discussions and calculations that took place during the week of the Study Group and soon afterwards. As such our consideration of both the experiment and the future for briquette-charged Persson and Bruff electrodes is incomplete, much remaining to be done. What is important is that we have shown that, using the models developed above, it seems possible to determine most of the qualitative details of the processes. Some uncertainties in the data (for example the paste viscosity) and the modelling have meant that accurate quantitative predictions are not yet available, but there seems to be no reason why this should not be possible in the near future. In particular, the modelling that has been carried out has led to the following conclusions:

- Paste flow and baking in both the experiment and the commercial (Persson and Bruff) electrodes may be modelled using an averaged two-phase slow flow approach. By formulating the models carefully from first principles the approximations inherent in the equations may be clearly enunciated.

- In both the experimental and industrial cases analysis has shown that a number of different regimes will probably be present. Different problems must be solved in each regime.

- No account has been taken so far of what happens in the final stages of the briquette recharging of electrodes when the pores in the melting paste close and air can no longer escape. This is likely to lead to complicated and involved modelling but is probably unlikely to materially affect predictions.

- The experiment may be modelled using various degrees of sophistication. More work is required regarding the effects of temperature variation, but predictions are broadly in line with experimental results.

- A two-dimensional time dependent well-posed model may be proposed for the Persson electrode. This would require a numerical solution, but of a fairly standard type.

- The time scales for both the experiment and the industrial electrode may be obtained.

- Whilst we have given little attention to the Bruff electrode, where the paste is melted and baked by heating provided by propane burners and the combustion of escaping paste hydrocarbons, it is clear that an inherent optimisation problem arises. If the heaters are not hot enough then an electrode with low strength and electrical conductivity will be produced. However, if the temperature of the heaters is too high not only will energy be wasted, but there is a danger of creating 'baked in' voids in the electrode.

- The feasibility of briquette charging for other electrode designs may be analysed using techniques similar to those developed here.

References

Drew, D.A. (1983) Mathematical modelling of two-phase flow, Ann. Rev. Fluid Mech. **15** 261-291.

Drew, D.A. & Wood, R.T. (1985) Overview and taxonomy of models and methods for workshop on two-phase flow fundamentals, National Bureau of Standards, Gaithersburg, Maryland.

Fulgenzi, C.F. (1992) New electrodes for arc furnaces, Proc. ABM Conf. Vitoria, Brazil.

Innvaer, R. (1992) A status for the Søderberg smelting electrode, VIE, Electrotech '92, Montreal, Canada.

Persson, J.A. & Fava, N.G. (1991) Silicon furnace technology, AIME Electric Furnace Conf. Proceedings, **49**, Toronto, Canada, 186-194.

Tørklep, K. (1988) Viscometry in paste production, Light Metals (Proc. AIME) 237-244.

Involved in problem: Jon Chapman, Paul Dellar, Don Drew, Alistair Fitt, Peter Howell, Sam Howison, John King, Clare Knock, Andrew Lacey, Dale Larson, Rafael Morones, Colin Please, Daniel Wheeler.

Report written by: ADF, PDH